Rapid Communications

Quantum interference between the optical Stark effect and resonant harmonic generation in WS_2

Darien J. Morrow, Daniel D. Kohler, Yuzhou Zhao, Jason M. Scheeler, Song Jin, and John C. Wright*
Department of Chemistry, University of Wisconsin–Madison, 1101 Avenue, Madison, Wisconsin 53706, USA

(Received 1 June 2020; accepted 11 September 2020; published 2 October 2020)

An applied field can modulate optical signals by resonance shifting via the Stark effect. The optical Stark effect uses ultrafast light in the transparency region of a material to shift resonances with speeds limited by the pulse duration or system coherence. In this Rapid Communication, we investigate the optical Stark effect in resonant optical harmonic generation using the A exciton transition of WS_2. Multidimensional pump-harmonic-probe measurements, in which the probe is second- or third-harmonic emission, reveal not only large Stark shifts that are commensurate with the large optical susceptibilities common to WS_2 excitons, but also behaviors more complex than simple optical Stark effect treatments predict. We show how another manifestation of the Stark effect, brought forth by coherent photon exchange between the pump and harmonic generation fundamental fields, can strongly enhance or suppress harmonic generation.

DOI: 10.1103/PhysRevB.102.161401

Optical harmonic generation (OHG) is an important light generation mechanism and a ubiquitous probe in microscopic analysis. Harmonic generation occurs when a strong light field E of frequency ω drives a nonlinear polarization that coherently radiates new light fields at the harmonics of the original frequency, $\{2\omega, 3\omega, \dots\}$ [Fig. 1(a)] [1,2]. Optical harmonic generation spectroscopy is sensitive to applied fields [3–6], and is a selective probe of semiconductor materials in ways complementary to that of traditional absorption and reflection probes [5,7–9].

A related optical process, also requiring strong light fields, is the optical Stark effect (OSE). In the optical Stark effect, a nonresonant optical pump creates photon-dressed states that hybridize with the system's original eigenstates, shifting their energies [Fig. 1(b)] by

$$\Delta E = \frac{|\mu_{ab}|^2 \mathcal{E}_{\text{pump}}^2}{E_0 - \hbar\omega_{\text{pump}}}, \tag{1}$$

in which $\mathcal{E}_{\text{pump}}$ is the field amplitude, μ_{ab} is the transition dipole between states a and b, and $E_0 \equiv E_b - E_a$ is the unpumped transition energy [10–13]. The optical Stark effect is well known in semiconductor exciton systems, but it is typically probed with a weak electric field [14–17].

The optical Stark effect can have an important interplay with optical harmonic generation. In resonant harmonic generation, the optical Stark effect alters resonance enhancement, which can modulate the harmonic generation efficiency [18,19]. Since the OSE is adiabatic, its ultrafast control of harmonic generation may suit photonics applications such as optical modulators [20]. The optical Stark effect also alters the free induction decay of the system, complicating pump-probe signals at the earliest pump-probe time delays and requiring careful attention to distinguish from absorption effects such as spectral hole burning [21–24]. These potential applications and effects motivate a study of the modification of optical harmonic generation by the optical Stark effect.

In this Rapid Communication, we connect the optical Stark effect to optical harmonic generation by exploring the IR pump, harmonic probe spectroscopy of WS_2. This OHG-probe spectroscopy is an example of the emerging methods which extend the capabilities of traditional pump-probe methods by using higher-order interactions for the pump and/or probe [8,9,25–28]. It is imperative to understand how the optical Stark effect influences this spectroscopy because processes such as charge separation at heterojunctions occur during pump-probe overlap [29]. The optical Stark effect and optical harmonic generation are pertinent for two-dimensional (2D) transition-metal dichalcogenides (TMDCs), where resonant optical transitions are generally strong [7,30–40]. Herein we show that the optical Stark effect is strong for optical harmonic generation, with resonance shift rates in excess of 2 meV per V/nm of applied optical field. In addition to the well-known optical Stark effect blueshift, we find the OSE-OHG process incurs different hybridization between the pump and probe fundamental fields. When the pump and the probe fundamental have similar frequencies, quantum interference [41] of the pump and probe photons strongly modulates the efficiency of harmonic generation. By tuning the pump frequency about the probe fundamental, the interference can either greatly suppress or enhance harmonic generation. The effect is similar to the recent photocurrent modulation using the interference of different multiphoton absorption processes [42–44].

Our experiments use two optical parametric amplifiers to generate linearly polarized pump and probe pulses [$\Delta_t \approx$ 50 fs full width at half maximum (FWHM)] (additional details are available in the Supplemental Material [45]). We measure second-harmonic generation (SHG) or third-harmonic generation (THG) of the probe beam [Fig. 1(c)] from a single WS_2 screw-dislocation spiral [84 nm tall, Figs. 1(d) and 1(e)] on a

*wright@chem.wisc.edu

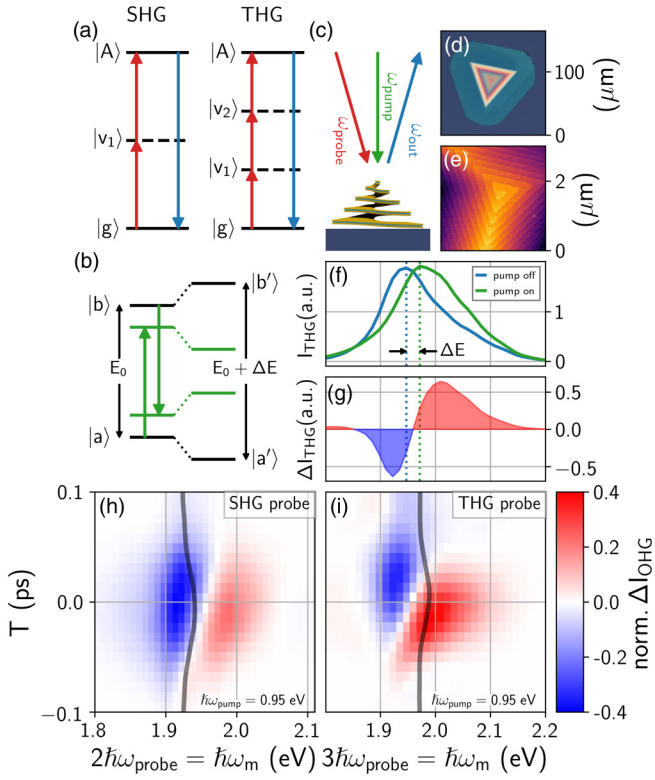

FIG. 1. Overview of the optical Stark effect and optical harmonic generation in WS_2. (a) Energy level diagrams with a probe (red) creating an A exciton coherence which then emits at a frequency (blue) which is a harmonic of the probe. (b) Nonresonant optical Stark effect in which a pump (green) drives the $a \leftrightarrow b$ transition which results in photon-dressed states with energy $E_0 + \Delta E$. (c) Illustration of the experimental geometry with $\omega_{\text{out}} = n\omega_{\text{probe}}$ and n being 2 for SHG and 3 for THG. (d, e) Optical and atomic force microscopy images of the WS_2 screw-dislocation pyramid on Si/SiO_2. (f) THG spectrum with NIR pump on and off. (g) Difference between THG spectra in (f). (h), (i) Difference between unpumped and pumped OHG spectrum [(h) SHG; (i) THG] for different pump-probe time delays T. The thick black lines are the center of mass of the pumped harmonic generation spectrum.

Si/SiO_2 substrate; we use a TMDC screw dislocation because it is known to have excellent nonlinear optical properties [46–49]. Figure 1(f) shows the A exciton THG resonance of the spiral (blue line). When a nonresonant pump (0.95 eV) is applied, the resonance blueshifts [Fig. 1(f), green line], yielding an asymmetric difference line shape [Fig. 1(g)].

To investigate the pump-OHG-probe, we measure the harmonic generation efficiency dependence on the pump and probe frequency, relative arrival time, and fluence. We look at changes in harmonic generation intensity relative to the peak of the unpumped harmonic generation spectrum,

$$\text{norm. } \Delta I \equiv \frac{I_{\text{OHG, pumped}} - I_{\text{OHG, unpumped}}}{\max\{I_{\text{OHG, unpumped}}\}}. \tag{2}$$

Figure 1(h) [Fig. 1(i)] shows the pump-SHG-probe (pump-THG-probe) spectrum as the pump-probe delay is scanned. The thick gray line traces the center of mass of the pumped resonance at the different pump-probe time delays T; the

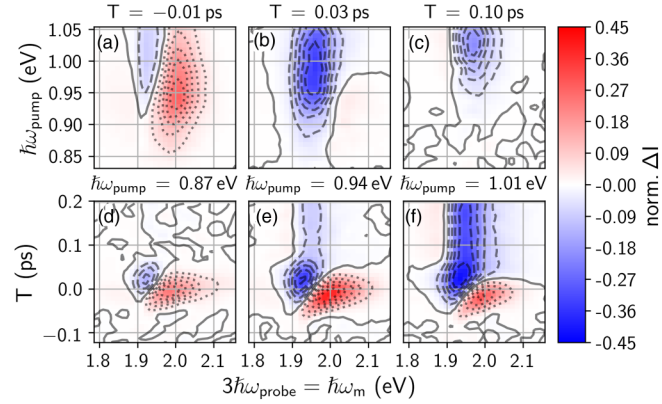

FIG. 2. Effects of pump frequency, probe frequency, and pump-probe time delay on WS_2 THG spectrum. (a)–(c) Pump frequency vs probe frequency for different time delays. (d)–(f) Time delay vs probe frequency for different pump frequencies. The color map is shared across all panels with contour lines locally normalized. $\mathcal{F}_{\text{pump}} \approx 3000\ \mu\text{J/cm}^2$.

pump blueshifts both SHG and THG with a time dependence that roughly follows the pump-probe temporal overlap. The nominal value of the SHG center of mass (e.g. $T = -0.1$ ps) shows that its resonance is shifted from that of the A exciton resonance. This difference in resonance frequency, along with the significantly weaker transition dipole (see the Supplemental Material [45]), suggests that the SHG resonance is not from the A exciton but perhaps a trion [3]. Henceforth we focus on THG of the A exciton.

Figure 2 shows the THG dependence on pump frequency $\hbar\omega_{\text{pump}}$, probe frequency $\hbar\omega_{\text{probe}}$, and pump-probe time delay T. When the probe arrives before the pump ($T < 0$), THG is enhanced near the resonance ($\Delta I > 0$). When pulses are overlapped ($T \approx 0$), the probe spectra (horizontal slices) are dispersive, which is consistent with blueshifting of the exciton resonance. When the probe is delayed by times greater than the pulse duration ($T > 50$ fs), the response is observed only when $2\hbar\omega_{\text{pump}} > E_0$, indicating that the pump is dissipating energy via two-photon absorption (2PA). The effects of absorption persist beyond 50 ps (see Fig. S15 in the Supplemental Material [45]).

Significantly, some of the pump-OHG-probe behaviors shown in Fig. 2 run counter to expectations from the conventional optical Stark effect. For example, the probe line shapes (horizontal slices of Fig. 2) are not strictly antisymmetric, contrary to expectations of a pure shift—this lack of strict antisymmetry is also seen in Fig. 1(g) in which the increase in THG to the blue of the resonance center frequency is greater in magnitude than the decrease in THG to the red of the resonance center [16,50,51]. The sizes of the positive (red) and negative (blue) lobes are unequal and depend on the pump color, and the dominant lobe differs between SHG (stronger negative) and THG (stronger positive) probes under the same pump excitation [cf. Figs. 1(h) and 1(i)]. Furthermore, the probe spectrum is strongly nonsymmetric about $T = 0$ [see Figs. 2(d)–(f)] which runs counter to the expectation of Eq. (1). These unusual behaviors cannot be explained by the incoherent population contributions

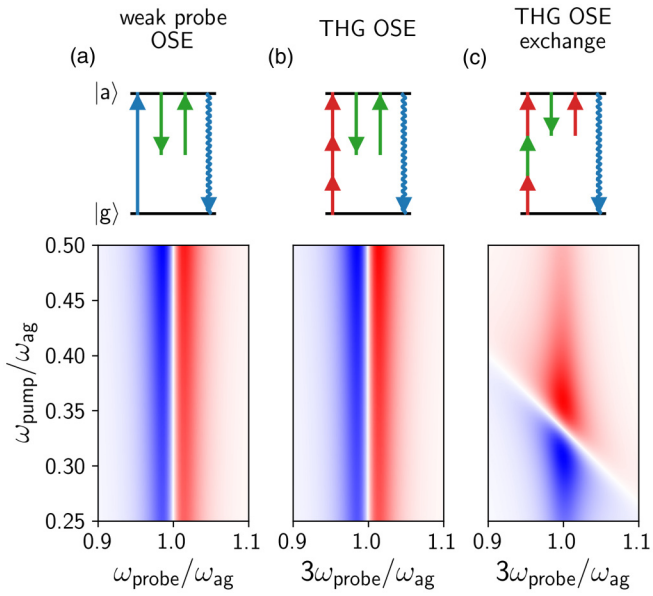

FIG. 3. Representations of the optical Stark effect using wave-mixing energy level (WMEL [53]) diagrams (first row) and their corresponding 2D frequency response (second row) at $T = 0$. Straight arrows represent interactions of the input fields: The resonant weak field probe (blue), the detuned pump (green), and the probe fundamental (red). The wavy blue arrow represents the emission of the signal field. Time flows from left to right. The 2D responses have a dephasing rate of $\Gamma = 0.025\omega_{ag}$ (see the Supplemental Material [45] for details).

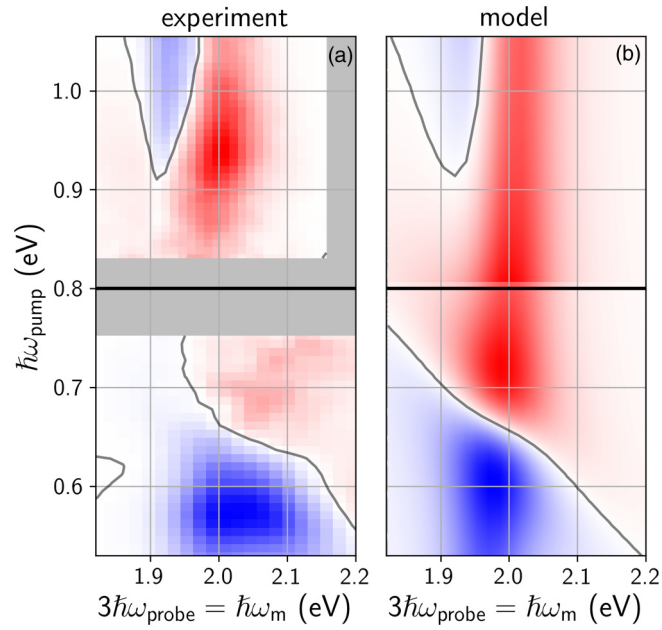

FIG. 4. Comparison between experiment and perturbative expansion model of the optical Stark effect for THG including finite pulse effects ($\hbar\omega_{ag} = 1.98$ eV, $\hbar\Gamma = 36$ meV $\Rightarrow T_2 = 18$ fs, and $\Delta_t = 50$ fs). Experimental data are for $T = -0.01$ ps. The upper and lower halves of (a) and (b) each have their own color map extent with red (blue) being an increase (decrease) in harmonic generation upon pump excitation. Data in (a) were normalized by the frequency-dependent pump intensity.

because these contributions are negligible for certain pump colors [Fig. 2(d)].

To understand the differences between the conventional optical Stark effect and its manifestation in optical harmonic generation, we employed the well-known perturbative expansion technique to a two-level system [13,52]. This expansion technique determines the nonlinear response through a series of coherent, time-ordered interactions with the pump and probe. Relevant diagrams are shown in Fig. 3 along with their $T = 0$ line shapes. Figure 3(a) shows the optical Stark effect in a transient absorption measurement and its pump-probe frequency response. The perturbative technique representation differs from Fig. 1(b) in that it does not explicitly solve for the hybridized states; it does, however, explicitly treat the probe polarization. Extension of the perturbative method to optical harmonic generation is trivial and discussed in the Supplemental Material [45].

The perturbative treatment recovers two processes that alter THG. The first is a direct optical Stark effect analog for THG [Fig. 3(b)], in which the third-harmonic polarization is dressed by the pump and the THG resonance blueshifts. In the second process [Fig. 3(c)], a triple-sum frequency (TSF [8], $\omega_{\mathrm{TSF}} = 2\omega_{\mathrm{probe}} + \omega_{\mathrm{pump}}$) polarization is dressed by the probe and pump fields. The process arises because the pump and probe have similar frequencies, so their roles in harmonic generation and dressing the system can exchange. This pathway's 2D spectrum can be understood as a blueshift of the $\omega_{\mathrm{TSF}} = \omega_{ag}$ TSF resonance, which explains the negatively sloped node. This manifestation of the optical Stark effect is unique to optical harmonic generation because in the weak probe case, degeneracy of the pump and probe frequencies implies the pump is at resonance, where incoherent excitation (carrier populations) or strong field Rabi cycling effects will dominate.

As derived in the Supplemental Material [45] [cf. Eq. (S79)], the net THG Stark effect is a weighted sum of the two Fig. 3 THG line shapes. The THG-OSE exchange is weighted three times larger than THG-OSE due to permutation symmetries of the pump and probe fields; for nth harmonic generation, there is an n-factor weighting. In effect, the optical Stark effect depends strongly on both pump and probe frequencies. When pump and probe frequencies differ greatly (e.g., $\omega_{\mathrm{pump}}/\omega_{ag} \approx 0.5$), the THG-OSE effect is clearly resolved, and a blueshift along the probe axis will result. Near pump-probe degeneracy, however, the exchange pathway is prevalent, and a blueshift normal to the TSF resonance is seen. Importantly, the blueshift from the exchange pathway enhances THG for $\omega_{\mathrm{pump}} > \omega_{\mathrm{probe}}$ and suppresses THG for $\omega_{\mathrm{pump}} < \omega_{\mathrm{probe}}$. This observation explains the spectral asymmetry of the OHG-OSE observed in both THG [e.g., Fig. 2(d)] and SHG [e.g., Fig. 1(h)].

Figure 4 compares a simulation of pump-THG-probe with the experiment. The simulation uses a numerical integration technique to account for a small pump-probe delay [54–56] and is similar to a weighted sum of the Fig. 3 THG line shapes. When the pump is well above degeneracy ($\hbar\omega_{\mathrm{pump}} \approx 1$ eV), the THG blueshift is clearly resolved. Crucially, when the probe and pump are scanned about degeneracy, the TSF

blueshift is clearly seen, an unambiguous confirmation of the THG-OSE exchange process.

Although this simulation shows the importance of the quantum interference between pathways, it only roughly reproduces the asymmetric dynamics about $T = 0$ (compare Fig. 2 to Figs. S8 and S9 in the Supplemental Material [45]). We believe this difference results because nonperturbative, higher-order effects must be taken into account to fully reproduce the dynamics in Figs. 2(d)–(f) [57]. Higher-order effects are evidenced in our data by the pump-induced 2PA and a probe-induced Stark effect (7 meV blueshift, Fig. S11 in the Supplemental Material [45]), indicating an eight-wave mixing formalism or higher is required to fully account for the asymmetric dynamics, which is a goal for future work.

Dissipative coupling of the pump, through multiphoton absorption, competes with the coherent optical Stark effect and gives the long-lived "bleach" signals clearly seen at delays longer than the pulse overlap, $T > 100$ fs. Multiphoton absorption is interesting for two opposing reasons: for pump-probe applications, it is a useful excitation mechanism because it reduces excitation pulse scatter [9]; for ultrafast modulation applications, it diminishes the time resolution from the optical Stark effect, so it may be a parameter to minimize. For optimizing ultrafast optical Stark effect modulation, it is beneficial to keep the pump color below the 2PA pump threshold $\hbar\omega_{\text{pump}} < E_0/2$ and close to pump and probe fundamental degeneracy, where the optical Stark effect exchange is enhanced. Our two-level model suggests contrast is also increased by using higher-order harmonics; as n increases, the relative contribution of the optical Stark effect exchange process increases (due to the number of pulse permutations), and the degeneracy point $\omega_{\text{pump}} = \omega_{\text{probe}} = \omega_{ag}/n$ occurs at frequencies well below the 2PA onset. This prediction holds when comparing SHG and THG; the SHG-OSE is hard to isolate because the resonance enhancement overlaps with the 2PA onset (see Fig. S10 in the Supplemental Material [45]). The OHG-OSE exchange process should also be strong for $n > 3$ and be sensitive to a wide variety of state symmetries through even versus odd harmonic orders [3,7,58]. For high enough harmonics, however, our description will break down because the mechanism of harmonic generation becomes nonperturbative [59,60].

To study how the pump fluence affects the optical Stark effect in harmonic generation, we tuned the pump to the 2PA threshold, ∼0.99 eV, and measured the change in THG for pump fluences of 500–7000 μJ/cm^2 (i.e., 1–20 V/nm) At the lowest fluence used, the signal is only seen near $T = 0$; the coherent, short-lived optical Stark effect dominates [Fig. 5(a)]. As expected for a multiphoton mechanism, however, the prominence of the population signal increases with increased pump fluence. At a sufficiently high fluence to suppress the majority (∼70%) of the THG resonance the persistent population signal is almost as large as the peak signals near $T = 0$ [Fig. 5(b)]. Figures 5(d) and 5(e) show the fluence scaling trends of the population and optical Stark effect signals. The optical Stark shift scales linearly with pump fluence as expected from Eq. (1). The population response [Fig. 5(e)] scales as $\mathcal{F}_{\text{pump}}^{1.4}$, while 2PA is expected to scale as $\mathcal{F}_{\text{pump}}^{2}$, or to saturate at high fluence. The discrepancy in

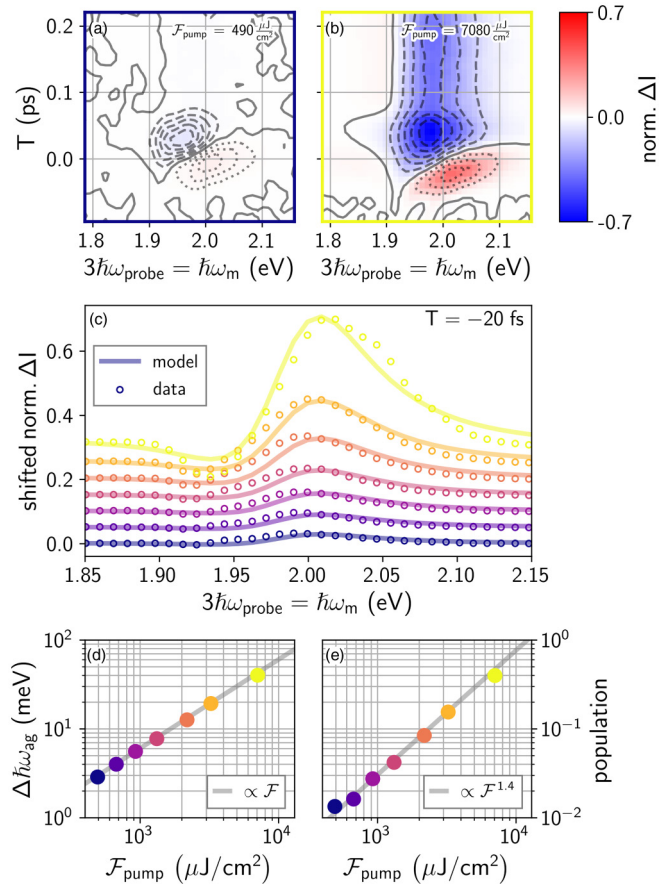

FIG. 5. Effects of pump fluence and pump-probe time delay on WS_2 THG spectrum when $\hbar\omega_{\text{pump}} = 0.99$ eV. (a), (b) Time delay vs probe frequency for pump fluences of 490 and 7080 μJ/cm^2 (contour lines are locally normalized). (c) $T = -20$ fs slices (color-keyed circles) at various pump fluences and fits (color-keyed lines) of the THG-OSE and THG-OSE exchange. (d) Fluence dependence of the Stark shift, $\Delta\hbar\omega_{ag} \equiv 1/2\,|\mu\mathcal{E}_{\text{pump}}|^2(\omega_{ag} - \omega_{\text{pump}})^{-1}$ [see Eq. (S80) in the Supplemental Material [45] for details]. (e) Population response (peak norm. ΔI amplitude after 0.1 ps) vs pump fluence.

scaling behavior is not understood, although the optical Stark effect is known to introduce surprising fluence scaling due to dynamic resonance conditions and broadening [19]. Our excitation density may also be large enough to modify intra- and interexciton forces, which would complicate the fluence scaling [61,62].

We also measured multidimensional pump-THG-probe in a variety of WS_2 morphologies to further investigate the balance of absorptive and coherent processes (see Figs. S11–S19 in the Supplemental Material [45]). We find that a crystalline monolayer exhibits a sharp 2PA pump color onset at $\hbar\omega_{\text{pump}} = E_0/2$, a narrow THG resonance, and roughly quadratic fluence scaling of the population. However, a polycrystalline thin film exhibits a broad 2PA pump color onset, a broad THG resonance, and roughly linear fluence scaling of the population. Other morphologies examined are in between these behaviors.

In this Rapid Communication we investigated both coherent and incoherent alteration of resonant harmonic generation in WS_2 from an intense, subband edge pump. The pump field not only shifts the resonant transition in a manner similar

to the traditional optical Stark effect with a single photon probe, but also exchanges with the probe field, resulting in another way to modulate harmonic generation. Perturbation theory adequately describes the multidimensional spectral and dynamic characteristics and will be essential for interpreting pump-OHG-probe spectra near the temporal overlap regime. The OHG-OSE exchange mechanisms may also have important applications in ultrafast photonic signal modulation.

All data and scripts used in this work are permissively licensed and available for reuse at the Open Science Framework [76].

We acknowledge support from the Department of Energy, Office of Basic Energy Sciences, Division of Materials Sciences and Engineering, under Award No. DE-FG02-09ER46664. D.J.M. acknowledges support from the Link Foundation.

[1] P. A. Franken, A. E. Hill, C. W. Peters, and G. Weinreich, Generation of Optical Harmonics, Phys. Rev. Lett. **7**, 118 (1961).

[2] P. D. Maker, R. W. Terhune, M. Nisenoff, and C. M. Savage, Effects of Dispersion and Focusing on the Production of Optical Harmonics, Phys. Rev. Lett. **8**, 21 (1962).

[3] K. L. Seyler, J. R. Schaibley, P. Gong, P. Rivera, A. M. Jones, S. Wu, J. Yan, D. G. Mandrus, W. Yao, and X. Xu, Electrical control of second-harmonic generation in a WSe_2 monolayer transistor, Nat. Nanotechnol. **10**, 407 (2015).

[4] C. Sirtori, F. Capasso, D. L. Sivco, A. L. Hutchinson, and A. Y. Cho, Resonant Stark tuning of second-order susceptibility in coupled quantum wells, Appl. Phys. Lett. **60**, 151 (1992).

[5] M. Lafrentz, D. Brunne, B. Kaminski, V. V. Pavlov, A. V. Rodina, R. V. Pisarev, D. R. Yakovlev, A. Bakin, and M. Bayer, Magneto-Stark Effect of Excitons as the Origin of Second Harmonic Generation in ZnO, Phys. Rev. Lett. **110**, 116402 (2013).

[6] D. Brunne, M. Lafrentz, V. V. Pavlov, R. V. Pisarev, A. V. Rodina, D. R. Yakovlev, and M. Bayer, Electric field effect on optical harmonic generation at the exciton resonances in GaAs, Phys. Rev. B **92**, 085202 (2015).

[7] G. Wang, X. Marie, I. Gerber, T. Amand, D. Lagarde, L. Bouet, M. Vidal, A. Balocchi, and B. Urbaszek, Giant Enhancement of the Optical Second-Harmonic Emission of WSe_2 Monolayers by Laser Excitation at Exciton Resonances, Phys. Rev. Lett. **114**, 097403 (2015).

[8] D. J. Morrow, D. D. Kohler, K. J. Czech, and J. C. Wright, Communication: Multidimensional triple sum-frequency spectroscopy of MoS_2 and comparisons with absorption and second harmonic generation spectroscopies, J. Chem. Phys. **149**, 091101 (2018).

[9] D. J. Morrow, D. D. Kohler, Y. Zhao, S. Jin, and J. C. Wright, Triple sum frequency pump-probe spectroscopy of transition metal dichalcogenides, Phys. Rev. B **100**, 235303 (2019).

[10] S. H. Autler and C. H. Townes, Stark effect in rapidly varying fields, Phys. Rev. **100**, 703 (1955).

[11] J. Bakos, AC Stark effect and multiphoton processes in atoms, Phys. Rep. **31**, 209 (1977).

[12] B. J. Sussman, Five ways to the nonresonant dynamic Stark effect, Am. J. Phys. **79**, 477 (2011).

[13] R. W. Boyd, *Nonlinear Optics*, 3rd ed. (Academic, New York, 2008).

[14] A. Mysyrowicz, D. Hulin, A. Antonetti, A. Migus, W. T. Masselink, and H. Morkoç, "Dressed Excitons" in a Multiple-Quantum-Well Structure: Evidence for an Optical Stark Effect with Femtosecond Response Time, Phys. Rev. Lett. **56**, 2748 (1986).

[15] N. Peyghambarian, S. W. Koch, M. Lindberg, B. Fluegel, and M. Joffre, Dynamic Stark Effect of Exciton and Continuum States in CdS, Phys. Rev. Lett. **62**, 1185 (1989).

[16] W. H. Knox, D. S. Chemla, D. A. B. Miller, J. B. Stark, and S. Schmitt-Rink, Femtosecond ac Stark Effect in Semiconductor Quantum Wells: Extreme Low- and High-Intensity Limits, Phys. Rev. Lett. **62**, 1189 (1989).

[17] R. Binder, S. W. Koch, M. Lindberg, N. Peyghambarian, and W. Schäfer, Ultrafast Adiabatic Following in Semiconductors, Phys. Rev. Lett. **65**, 899 (1990).

[18] M. Holthaus and D. W. Hone, AC Stark effects and harmonic generation in periodic potentials, Phys. Rev. B **49**, 16605 (1994).

[19] J. Elgin and G. New, Semi-classical theory of two-photon resonant third-harmonic generation, Opt. Commun. **16**, 242 (1976).

[20] Z. Sun, A. Martinez, and F. Wang, Optical modulators with 2D layered materials, Nat. Photonics **10**, 227 (2016).

[21] C. B. Cruz, J. Gordon, P. Becker, R. Fork, and C. Shank, Dynamics of spectral hole burning, IEEE J. Quantum Electron. **24**, 261 (1988).

[22] B. Fluegel, N. Peyghambarian, G. Olbright, M. Lindberg, S. W. Koch, M. Joffre, D. Hulin, A. Migus, and A. Antonetti, Femtosecond Studies of Coherent Transients in Semiconductors, Phys. Rev. Lett. **59**, 2588 (1987).

[23] M. Joffre, D. Hulin, A. Migus, A. Antonetti, C. B. a. la Guillaume, N. Peyghambarian, M. Lindberg, and S. W. Koch, Coherent effects in pump–probe spectroscopy of excitons, Opt. Lett. **13**, 276 (1988).

[24] S. Schmitt-Rink, D. S. Chemla, and H. Haug, Nonequilibrium theory of the optical Stark effect and spectral hole burning in semiconductors, Phys. Rev. B **37**, 941 (1988).

[25] W. Xiong, J. E. Laaser, P. Paoprasert, R. A. Franking, R. J. Hamers, P. Gopalan, and M. T. Zanni, Transient 2D IR spectroscopy of charge injection in dye-sensitized nanocrystalline thin films, J. Am. Chem. Soc. **131**, 18040 (2009).

[26] D. R. Dietze and R. A. Mathies, Femtosecond stimulated Raman spectroscopy, ChemPhysChem **17**, 1224 (2016).

[27] A. Mandal, J. D. Schultz, Y.-L. Wu, A. F. Coleman, R. M. Young, and M. R. Wasielewski, Transient two-dimensional electronic spectroscopy: Coherent dynamics at arbitrary times along the reaction coordinate, J. Phys. Chem. Lett. **10**, 3509 (2019).

[28] F. Langer, C. P. Schmid, S. Schlauderer, M. Gmitra, J. Fabian, P. Nagler, C. Schüller, T. Korn, P. G. Hawkins, J. T. Steiner, U. Huttner, S. W. Koch, M. Kira, and R. Huber, Lightwave valleytronics in a monolayer of tungsten diselenide, Nature (London) **557**, 76 (2018).

[29] X. Hong, J. Kim, S.-F. Shi, Y. Zhang, C. Jin, Y. Sun, S. Tongay, J. Wu, Y. Zhang, and F. Wang, Ultrafast charge transfer in atomically thin MoS_2/WS_2 heterostructures, Nat. Nanotechnol. **9**, 682 (2014).

[30] E. J. Sie, J. W. McIver, Y.-H. Lee, L. Fu, J. Kong, and N. Gedik, Valley-selective optical Stark effect in monolayer WS_2, Nat. Mater. **14**, 290 (2014).

[31] E. J. Sie, C. H. Lui, Y.-H. Lee, J. Kong, and N. Gedik, Observation of intervalley biexcitonic optical Stark effect in monolayer WS_2, Nano Lett. **16**, 7421 (2016).

[32] E. J. Sie, C. H. Lui, Y.-H. Lee, L. Fu, J. Kong, and N. Gedik, Large, valley-exclusive Bloch-Siegert shift in monolayer WS_2, Science **355**, 1066 (2017).

[33] J. Kim, X. Hong, C. Jin, S.-F. Shi, C.-Y. S. Chang, M.-H. Chiu, L.-J. Li, and F. Wang, Ultrafast generation of pseudo-magnetic field for valley excitons in WSe_2 monolayers, Science **346**, 1205 (2014).

[34] C.-K. Yong, J. Horng, Y. Shen, H. Cai, A. Wang, C.-S. Yang, C.-K. Lin, S. Zhao, K. Watanabe, T. Taniguchi, S. Tongay, and F. Wang, Biexcitonic optical Stark effects in monolayer molybdenum diselenide, Nat. Phys. **14**, 1092 (2018).

[35] C.-K. Yong, M. I. B. Utama, C. S. Ong, T. Cao, E. C. Regan, J. Horng, Y. Shen, H. Cai, K. Watanabe, T. Taniguchi, S. Tongay, H. Deng, A. Zettl, S. G. Louie, and F. Wang, Valley-dependent exciton fine structure and Autler–Townes doublets from Berry phases in monolayer $MoSe_2$, Nat. Mater. **18**, 1065 (2019).

[36] T. LaMountain, H. Bergeron, I. Balla, T. K. Stanev, M. C. Hersam, and N. P. Stern, Valley-selective optical Stark effect probed by Kerr rotation, Phys. Rev. B **97**, 045307 (2018).

[37] P. D. Cunningham, A. T. Hanbicki, T. L. Reinecke, K. M. McCreary, and B. T. Jonker, Resonant optical Stark effect in monolayer WS_2, Nat. Commun. **10**, 5539 (2019).

[38] Y. Li, Y. Rao, K. F. Mak, Y. You, S. Wang, C. R. Dean, and T. F. Heinz, Probing symmetry properties of few-layer MoS_2 and h-BN by optical second-harmonic generation, Nano Lett. **13**, 3329 (2013).

[39] L. M. Malard, T. V. Alencar, A. P. M. Barboza, K. F. Mak, and A. M. de Paula, Observation of intense second harmonic generation from MoS_2 atomic crystals, Phys. Rev. B **87**, 201401(R) (2013).

[40] R. Wang, H.-C. Chien, J. Kumar, N. Kumar, H.-Y. Chiu, and H. Zhao, Third-harmonic generation in ultrathin films of MoS_2, ACS Appl. Mater. Interfaces **6**, 314 (2013).

[41] K.-Q. Lin, S. Bange, and J. M. Lupton, Quantum interference in second-harmonic generation from monolayer WSe_2, Nat. Phys. **15**, 242 (2019).

[42] K. Wang, R. A. Muniz, J. E. Sipe, and S. T. Cundiff, Quantum Interference Control of Photocurrents in Semiconductors by Nonlinear Optical Absorption Processes, Phys. Rev. Lett. **123**, 067402 (2019).

[43] P. T. Mahon, R. A. Muniz, and J. E. Sipe, Quantum interference control of localized carrier distributions in the Brillouin zone, Phys. Rev. B **100**, 075203 (2019).

[44] R. A. Muniz, C. Salazar, K. Wang, S. T. Cundiff, and J. E. Sipe, Quantum interference control of carriers and currents in zinc blende semiconductors based on nonlinear absorption processes, Phys. Rev. B **100**, 075202 (2019).

[45] See Supplemental Material at http://link.aps.org/supplemental/10.1103/PhysRevB.102.161401 for materials and methods, a unified perturbation theory of the optical Stark effect for weak field and harmonic probes, additional numerical simulations of pump-THG-probe, comparison of pump-SHG-probe and our optical Stark effect theory, demonstration of probe-induced optical Stark effect, and additional pump-THG-probe measurements on various WS_2 morphologies, which includes Refs. [3,8–10,13,15,21,23,31,34,37,46,52,54,63–75].

[46] Y. Zhao and S. Jin, Controllable water vapor assisted chemical vapor transport synthesis of WS_2-MoS_2 heterostructure, ACS Mater. Lett. **2**, 42 (2020).

[47] M. J. Shearer, L. Samad, Y. Zhang, Y. Zhao, A. Puretzky, K. W. Eliceiri, J. C. Wright, R. J. Hamers, and S. Jin, Complex and noncentrosymmetric stacking of layered metal dichalcogenide materials created by screw dislocations, J. Am. Chem. Soc. **139**, 3496 (2017).

[48] X. Fan, Y. Jiang, X. Zhuang, H. Liu, T. Xu, W. Zheng, P. Fan, H. Li, X. Wu, X. Zhu, Q. Zhang, H. Zhou, W. Hu, X. Wang, L. Sun, X. Duan, and A. Pan, Broken symmetry induced strong nonlinear optical effects in spiral WS_2 nanosheets, ACS Nano **11**, 4892 (2017).

[49] X. Fan, Y. Zhao, W. Zheng, H. Li, X. Wu, X. Hu, X. Zhang, X. Zhu, Q. Zhang, X. Wang, B. Yang, J. Chen, S. Jin, and A. Pan, Controllable growth and formation mechanisms of dislocated WS_2 spirals, Nano Lett. **18**, 3885 (2018).

[50] Y. Yang, M. Yang, K. Zhu, J. C. Johnson, J. J. Berry, J. van de Lagemaat, and M. C. Beard, Large polarization-dependent exciton optical Stark effect in lead iodide perovskites, Nat. Commun. **7**, 12613 (2016).

[51] A. H. Proppe, G. W. Walters, A. Y. Alsalloum, A. A. Zhumekenov, E. Mosconi, S. O. Kelley, F. D. Angelis, L. Adamska, P. Umari, O. M. Bakr, and E. H. Sargent, Transition dipole moments of $n = 1$, 2, and 3 perovskite quantum wells from the optical Stark effect and many-body perturbation theory, J. Phys. Chem. Lett. **11**, 716 (2020).

[52] S. Mukamel, *Principles of Nonlinear Optical Spectroscopy* (Oxford University Press, Oxford, UK, 1999).

[53] D. Lee and A. C. Albrecht, A unified view of Raman, resonance Raman, and fluorescence spectroscopy (and their analogues in two-photon absorption), in *Advances in Infrared and Raman Spectroscopies*, edited by R. J. H. Clark and R. E. Hester, Vol. 12 (Wiley, New York, 1985), pp. 179–213.

[54] D. D. Kohler, B. J. Thompson, and J. C. Wright, Frequency-domain coherent multidimensional spectroscopy when dephasing rivals pulsewidth: Disentangling material and instrument response, J. Chem. Phys. **147**, 084202 (2017).

[55] M. F. Gelin, D. Egorova, and W. Domcke, Efficient method for the calculation of time- and frequency-resolved four-wave mixing signals and its application to photon-echo spectroscopy, J. Chem. Phys. **123**, 164112 (2005).

[56] B. Thompson, K. Sunden, and D. Kohler, WrightSim, https://doi.org/10.5281/zenodo.3774515 (2020).

[57] O. Blum, P. Harshman, T. K. Gustafson, and P. L. Kelley, Application of radiative renormalization to strong-field resonant nonlinear optical interactions, Phys. Rev. A **47**, 5165 (1993).

[58] Z. Ye, T. Cao, K. O'Brien, H. Zhu, X. Yin, Y. Wang, S. G. Louie, and X. Zhang, Probing excitonic dark states in

single-layer tungsten disulphide, Nature (London) **513**, 214 (2014).

[59] H. Liu, Y. Li, Y. S. You, S. Ghimire, T. F. Heinz, and D. A. Reis, High-harmonic generation from an atomically thin semiconductor, Nat. Phys. **13**, 262 (2016).

[60] S. Ghimire and D. A. Reis, High-harmonic generation from solids, Nat. Phys. **15**, 10 (2019).

[61] A. Chernikov, C. Ruppert, H. M. Hill, A. F. Rigosi, and T. F. Heinz, Population inversion and giant bandgap renormalization in atomically thin WS_2 layers, Nat. Photonics **9**, 466 (2015).

[62] E. J. Sie, A. Steinhoff, C. Gies, C. H. Lui, Q. Ma, M. Rösner, G. Schönhoff, F. Jahnke, T. O. Wehling, Y.-H. Lee, J. Kong, P. Jarillo-Herrero, and N. Gedik, Observation of exciton redshift–blueshift crossover in monolayer WS_2, Nano Lett. **17**, 4210 (2017).

[63] K. J. Czech, B. J. Thompson, S. Kain, Q. Ding, M. J. Shearer, R. J. Hamers, S. Jin, and J. C. Wright, Measurement of ultrafast excitonic dynamics of few-layer MoS_2 using state-selective coherent multidimensional spectroscopy, ACS Nano **9**, 12146 (2015).

[64] K. Furuta, M. Fuyuki, and A. Wada, Cross-term selective, two-pulse correlation measurements by phase-shifted parallel modulation for analysis of a multi-photon process, Appl. Spectrosc. **66**, 1475 (2012).

[65] B. Thompson, K. Sunden, D. Morrow, D. Kohler, and J. Wright, WrightTools: A Python package for multidimensional spectroscopy, J. Open Source Softw. **4**, 1141 (2019).

[66] P. Virtanen, R. Gommers, T. E. Oliphant, M. Haberland, T. Reddy, D. Cournapeau, E. Burovski, P. Peterson, W. Weckesser, J. Bright, S. J. van der Walt, M. Brett, J. Wilson, K. J. Millman, N. Mayorov, A. R. J. Nelson, E. Jones, R. Kern, E. Larson, C. J. Carey *et al.*, SciPy 1.0: Fundamental algorithms for scientific computing in Python, Nat. Methods **17**, 261 (2020).

[67] S. van der Walt, S. C. Colbert, and G. Varoquaux, The NumPy array: A structure for efficient numerical computation, Comput. Sci. Eng. **13**, 22 (2011).

[68] J. D. Hunter, Matplotlib: A 2D graphics environment, Comput. Sci. Eng. **9**, 90 (2007).

[69] C. Cohen-Tannoudji and S. Reynaud, Dressed-atom description of resonance fluorescence and absorption spectra of a multi-level atom in an intense laser beam, J. Phys. B **10**, 345 (1977).

[70] E. Jaynes and F. Cummings, Comparison of quantum and semiclassical radiation theories with application to the beam maser, Proc. IEEE **51**, 89 (1963).

[71] B. R. Mollow, Power spectrum of light scattered by two-level systems, Phy. Rev. **188**, 1969 (1969).

[72] P. Hamm and M. Zanni, *Concepts and Methods of 2D Infrared Spectroscopy* (Cambridge University Press, Cambridge, UK, 2011).

[73] C. Sieh, T. Meier, F. Jahnke, A. Knorr, S. W. Koch, P. Brick, M. Hübner, C. Ell, J. Prineas, G. Khitrova, and H. M. Gibbs, Coulomb Memory Signatures in the Excitonic Optical Stark Effect, Phys. Rev. Lett. **82**, 3112 (1999).

[74] M. Lindberg and S. W. Koch, Theory of coherent transients in semiconductor pump–probe spectroscopy, J. Opt. Soc. Am. B **5**, 139 (1988).

[75] J. P. Sokoloff, M. Joffre, B. Fluegel, D. Hulin, M. Lindberg, S. W. Koch, A. Migus, A. Antonetti, and N. Peyghambarian, Transient oscillations in the vicinity of excitons and in the band of semiconductors, Phys. Rev. B **38**, 7615 (1988).

[76] D. Morrow, Quantum interference between the optical Stark effect and resonant harmonic generation in WS_2, http://dx.doi.org/10.17605/OSF.IO/SNTPC (2020).